Fine-crushing and subcritical water treatment of wood materials suitable for bioethanol production using image processing as intermediate indicators

Yamaguchi, Daizo ; Hatano, Akishi ; Shoji, Koichi ; Itoh, Hiromichi ; Kawamura, Tsuneo ; Horio, Hisashi

(Citation)
Biosystems Engineering,101(4):436-444

(Issue Date)
2008-10

(Resource Type)
journal article

(Version)
Accepted Manuscript

(URL)
https://hdl.handle.net/20.500.14094/90000981

Fine-crushing and subcritical water treatment of wood materials suitable for bioethanol production using image processing as intermediate indicators

Daizo Yamaguchi[a,*], Akishi Hatano[b],
Koichi Shoji[c], Hiromichi Itho[c], Tsuneo Kawamura[c], Hisashi Horio[c]

[a]Graduate School of Science and Technology, Kobe University, Present address: KANAGAWA ACADEMY OF SCIENCE AND TECHNOLOGY, KSP East 309, 3-2-1 Sakado, Takatsu-ku, Kawasaki-shi, Kanagawa, 213-0012, Japan

[b]Graduate School of Science and Technology, Kobe University, Present address: NTT DATA CORPORATION, Toyosu Center Building, 3-3, Toyosu 3-chome, Koto-ku, Tokyo 135-6033, Japan

[c]Graduate School of Agriculture, Kobe University, 1-1 Rokkodai-cho, Nada-ku, Kobe, 657-8501, Japan

[*]Corresponding author. Kanagawa Academy of Science and Technology, KSP East 309, 3-2-1 Sakado, Takatsu-ku, Kawasaki-shi, Kanagawa, 213-0012, Japan. Tel.: +81 44 819 2044; fax: +81 44 819 2039. E-mail address: hp_yamaguchi@newkast.or.jp (D. Yamaguchi).

Abstract

In the production of ethanol from woody materials through enzymatic saccharification, the prerequisite is the removal of lignin for converting cellulose into monosaccharide. Producing fine-crushed material by a fine-crusher, quantitatively evaluating its shape or surface texture by an image analysis, and

subjecting it to subcritical water treatment constitute a new preprocessing technology for the removal of lignin. The image analysis revealed that fine-crushing for exposing the wood fibre results in a high removal of lignin. The exposure of wood fibre increased with increasing the moisture content of material. The most favourable fine-crushed material for subcritical water treatment was produced by the use of a small pore size of punching sieve and a high moisture content of material.

Notation

ASM: angular second moment

C: contrast

IE: information entropy

r: distance separated by two neighbouring pixels

θ: angle separated by two neighbouring pixels

CM: average of contrast

CV: variance of contrast

i: rows in the co-occurrence matrix

j: column in the co-occurrence matrix

$P_{r,\theta}(i,j)$: (*i*-th, *j*-th) entry in a normalized co-occurrence probability matrix

FD: fractal dimension

δ: proper separation length with the image divided into a rectangular lattice

N_δ: number of the boxes including the outline

LRI: lignin removal index, %

M: mass of material before subcritical water treatment, g

M': mass of material after subcritical water treatment, g

L: Klason lignin of the sample after subcritical water treatment, %

L_0: Klason lignin of smashed material before the subcritical water treatment, %

S: mass of material before the Klason procedure, g

W: mass of material after the Klason procedure, g

R^2_{adj}: squared multiple correlation coefficients adjusted for the degrees of freedom

1. Introduction

Enzymatic hydrolysis, an alternative to acid hydrolysis, of lignocellulosic material is a promising next-generation method for the effective production of ethanol, although obstacles such as end-product inhibition of cellulase activity need to be overcome (Sun and Cheng, 2002). The enzyme issue can be surmounted by the use of a novel cellulose-degrading yeast strain that genetically releases cellulolytic enzymes on the surface of yeast cells (Fujita et al., 2002, 2004), allowing direct fermentation of wood cellulose into ethanol. The yeast displaying several types of cellulase on the surface overcomes the end-product inhibition of cellulase activity because monosaccharides are immediately converted into ethanol by the yeast.

Even with the use of such novel yeast, however, the lignin must inevitably be removed to expose the cellulose and to activate the cellulase enzymes while obviating the production of 5-hydroxymethyl-2-furfural, an inhibitor of ethanol fermentation by the yeast. The presence of lignin complicates the access of cellulase enzymes to cellulose and reduces the efficiency of the hydrolysis, necessitating an efficient preprocessing technology for enzymatic hydrolysis of woody material.

Sun and Cheng (2002) have reviewed several types of hydrolysis of lignocellulosic materials for ethanol production and have indicated the importance of preprocessing the lignocellulosic materials before enzymatic hydrolysis to remove lignin for efficient hydrolysis of cellulose. Gregg et al. (1998) have also shown that removal and recovery of lignin are the main contributors to the cost of producing the ethanol. Physical (mechanical comminution, pyrolysis), physico-chemical (steam explosion, ammonia fibre explosion), chemical (ozonolysis, acid hydrolysis, alkaline hydrolysis), and biological processes have been developed for preprocessing lignocellulosic materials (Matsumura et al., 1977; Magara et al., 1988; Sun and Cheng, 2002; Forestry and Forest Products Research Institute, 2004; Hayashi et al., 2004). These methods have yet to lead to practical application, however. Concentrated attempts have been made at physical and chemical degrading: small (10-30 μm) vibration-ground materials expose a large total surface area, which affects the hydrolysis rate by increasing enzymatic susceptibility (Matsumura et al. 1977); the degradation rate of holocellulose by enzymes increases when lignin is removed (60% from hardwood) by the acid chlorite procedure (Sudo et al. 1976). Nonetheless, the former requires high energy for grinding the wood material, and the latter needs chemical agents, heat and treatment of liquid wastes. Both methods need to become cost-effective for industrialization.

The combination of fine-crushing woody material by a fine-crusher and subjecting it to subcritical water treatment is one of the promising techniques for removing lignin. Studies on a newly developed light-weight, low-energy-consuming fine-crusher have demonstrated that the pore size of the punching sieve and the moisture content of the material affect the shape of

fine-crushed wood, where fractal dimension and weighted average diameter of the fine-crushed material are negatively correlated with each other (Yamaguchi et al., 2004, 2006). Subcritical water has unique properties in relation to the ion product, dielectric constant, viscosity, diffusivity, density, electric conductance, and solvent ability. One of the major reactions in subcritical water treatment is hydrolysis. The ion product and dielectric constant therefore play important roles (Goto et al., 2004) and, consequently, it functions as an acid and/or alkali catalyst by facilitating rapid degradation of the lignin, the hemicellulose and the cellulose. It is worth stating that subcritical water itself is a neutral medium to the environment, with regard to waste treatment during the production.

Since the reaction of subcritical water with wood material occurs on the wood surface, evaluation of the shape or surface of wood material is considered to be significantly important. Accordingly, we have applied image processing for this quantitative evaluation. The image processing step enables direct evaluation of the shape of the fine-crushed material by a simple method without microscopic observation, and provides an index of the fine-crushing process ahead of subcritical water treatment.

The objectives of the present study are: (1) to determine by image analysis the significant characteristics of fine-crushed wood for effective lignin removal, (2) to optimize the performance of the fine-crusher for obtaining optimal wood characteristics.

2. Materials and methods

2.1. *Fine-crusher and material*

The fine crusher consisted of a flail-knife rotor and a circular- or

elliptical-pore rotary sieve, both rotating on a common shaft driven by 5.5 kW and 1.5 kW inverter motors, respectively (Yamaguchi et al., 2004; 2006). It was covered with a casing leading to a cyclone separator, and most of the fine-crushed material was collected in drawers set at the base of the casing. The wood material used was naturally dried Chinese elm (*Ulmus parvifolia*), coarse-crushed with a 4.5 kW chopper.

2.2. *Image processing*

A sample of the fine-crushed wood placed in a 60×80mm frame was digitally photographed at a distance of 200 mm. Under a long exposure time (0.25 s) and additional lighting, a substantial depth of the field was maintained at an exposure of F9.9 to avoid unfocused regions in the image. The average of 9 images of each sample was used as data.

The image was processed as described in Figure 1. Adobe Photoshop^{TM} was used to extract the image data (Fig. 1 a). Subsequent processing was carried out by a C language program. The brightness of each pixel of the image (*MN*) was obtained as follows:

$$MN = 0.300R + 0.59G + 0.11B \quad (1)$$

where *R*, *G*, *B* are 8-bit luminance intensities of each pixel on red, green, and blue planes (Fig. 1 b), respectively.

Fourteen features (Haralick et al. 1973) indicated below and derived from the co-occurrence matrixes (Bodun et al., 2000) were obtained from red, green, blue, and brightness images. The angular second moment $ASM(r,\theta)$, the contrast $C(r,\theta)$, and the information entropy $IE(r,\theta)$, were calculated by equations (2) to (4) at θ as 0˚, 45˚, 90˚, 135˚, r = 1 ($r = \sqrt{2}$ at θ = 45˚, 135˚), respectively, where (r,θ) is the coordinate of the pixels: r is the distance between two

neighbouring pixels and θ is the angle between two neighbouring pixels (Haralick et al. 1973; Image Processing Handbook Edit Committee, 1987).

$$ASM(r,\theta) = \sum_i \sum_j \{P_{r,\theta}(i,j)\}^2 \quad (2)$$

$$C(r,\theta) = \sum_i \sum_j (i-j)^2 P_{r,\theta}(i,j) \quad (3)$$

$$IE(r,\theta) = -\sum_i \sum_j P_{r,\theta}(i,j)\{P_{r,\theta}(i,j)\} \quad (4)$$

where i and j are the rows and column in the co-occurrence matrix, and $P_{r,\theta}(i,j)$ is (i,j) (i-th, j-th) entry in a normalized co-occurrence probability (Bodun et al., 2000). The average CM and variance CV of the contrast were also calculated as shown in equations (5) and (6) below.

$$CM = \frac{1}{n}\sum_\theta C(r,\theta) \quad (5)$$

$$CV = \frac{1}{n}\sum_\theta \{C(r,\theta) - CM\}^2 \quad (6)$$

where, n the number of the angles θ (0˚, 45˚, 90˚, 135˚ and therefore, n=4 in the present study). The angular second moment measures the luminance intensity that determines relative smoothness; a zero value represents the highest level of spatial non-homogeneity, and a value of 1 indicates a constant or equal magnitude over the image region. The contrast measures the degree of variation where a zero-value denotes no contrast, while larger values correspond to an increase in contrast or coarseness. The information entropy determines the degree of randomness or lack of information contained in the co-occurrence matrix (Bodun et al., 2000).

The fractal dimensions (*FD*) for red, green, blue and brightness images were calculated by the box-count algorithm (Hatano et al., 2002, Honda, 2002, Yamaguchi et al., 2006).

$$FD = -\frac{\log N_\delta}{\log \delta} \quad (7),$$

where δ is the proper separation length with the image divided into a rectangular lattice, and N_δ the number of boxes including the outline. The outline was extracted by gradient as edge enhancement (Fig. 1 c) and the binarisation was carried out at threshold level of 150 out of 256 (8-bit) (Fig. 1 d). Image denoising was not carried out.

2.3. *Subcritical water treatment and lignin content measurement*

The apparatus for subcritical water treatment included a PID controller. An autoclave (35 ml) was surrounded by a heater and sealed with an O-ring and connectors. Wood-water slurry (a mixture of fine-crushed material and ion-exchanged water) was placed in the autoclave. The internal temperature of the autoclave was detected by a sheath thermocouple inserted from the connector and was controlled by the PID controller. The desired temperature was set on the controller, and the internal temperature was stored into a data logger.

The wood-water slurry placed in the autoclave was subjected to subcritical water treatment. The volume of slurry, the significant factor associated with treatment pressure, was maintained at 30 ml to control its concentration. The duration of treatment was varied and defined as the time elapsed excluding the first 500 s needed to raise the temperature. The autoclave was then cooled, and the slurry was separated into liquid and solid parts through a 1G-4 filter. The solid part was used for measuring the lignin by the 72 % sulfuric acid method

(Klason Method) after the extraction of soluble organic parts (The Japan Wood Research Society, 2000).

The lignin removal index (*LRI*) (the effect of subcritical water treatment) was defined and calculated as follows:

$$LRI = 1 - \frac{M'}{M}\frac{L}{L_0} \quad (8),$$

where M and M' are the mass of material before and after the subcritical water treatment, L the Klason lignin (acid-insoluble lignin) of the sample (Eq. 9) after subcritical water treatment and L_0 the Klason lignin of smashed material before the subcritical water treatment (30.4%).

$$L = \frac{W}{S} \quad (9)$$

where S and W are the mass of material before and after the Klason procedure (The Japan Wood Research Society, 2000). Klason lignin of smashed material before the subcritical water treatment L_0 was similarly calculated.

In the Klason Method, cellulose and hemicellulose are hydrolyzed by 72 % (v/v) sulfuric acid, and the acid-insoluble lignin is measured as W. When the cellulose and hemicellulose are not sufficiently hydrolyzed (e.g. the size of the tested material is too large for the sulfuric acid to penetrate), however, the *LRI* may take a negative value because L becomes larger than L_0.

2.4. *Electron microscope analysis*

The microscopic shape of fine-crushed material affecting the *LRI* was examined under a scanning electron microscope (SEM) set at an accelerating voltage of 15 kV, a working distance of 20 mm, and a spot size of 20 or 40 μm.

3. Designs of experiment and procedures

3.1. *Determination of significant image characteristics of fine-crushed material related to removal of lignin.*

The driving conditions of the fine-crusher to produce fine-crushed material are shown in Table 1. Image analysis and subcritical water treatment were replicated twice on material from different trees of the same species; Klason lignin of smashed material before subcritical water treatment (L_0) were 28.8% and 30.4% for replicates I and II, respectively. In the subcritical water treatments, five grams of wood material and 30 ml of distilled water were placed into the autoclave and heated at 200 ºC for 5 minutes.

Outliers in the experimental data were checked by the jackknife method. To select the optimal image characteristics of fine-crushed material for the estimation of lignin removal by subcritical water treatment, first, decorrelation between *LRI* and image characteristics was checked for efficient subsequent analysis; the statistically insignificant data were not taken into consideration. The relation between the *LRI* and the image characteristics of the fine-crushed material was then analyzed by the multiple linear regression method (Valero et al., 2004; Pasini et al., 2004; Canneyt, et al., 2004; Sinício, 2004; Jain and Pathare, 2004). The data were standardized prior to the analysis, and stepwise selection was applied to the multiple linear regression analysis. Multicolinearity was checked by the variance inflation factor. The significance was tested of the regression formula (F-test) and the standardized partial regression coefficients (two-sided t-test).

3.2. *Driving conditions of fine-crusher to achieve optimal image characteristics.*

The fine-crushed material obtained from the previous study (Yamaguchi et al., 2006) (using the orthogonal array L_{27}) were used, and further image analyses were conducted (Table 2). The relation between the selected image characteristics of fine-crushed material and the conditions of the fine-crusher was also analyzed by the multiple linear regression method in the same manner. Images were also digitally photographed at distances of 200 and 135 mm.

4. Results and discussion

4.1. *Image characteristics*

The *LRI* obtained from subcritical water treatment is shown in Table 1. The jackknife method disclosed an outlier of 9.6% in the *LRI* (Table 1), which was not taken into consideration. The multiple linear regressions analyses (Table 3) demonstrated that the *FD* of the green image of the circular sieve and the angular second moment (135˚) (ASM_{135}) of the brightness image of the elliptical sieve were statistically the optimal characteristics for the estimation of *LRI*. Although both models were simple linear regression, R^2_{adj} were sufficiently high with a significance level of 0.1%. The plus or minus sign in the regression coefficients (Table 3) agreed with the definition of *FD* or ASM_{135}, where *FD* positively correlates to the complexity of the contour and ASM_{135} negatively to that in spatial non-homogeneity of the fine-crushed material. These complexities of the shape of fine-crushed material contributed favourably to the removal of lignin during the subcritical water treatment.

One possible explanation for the difference in the selected characteristics between the circular and elliptical sieves is the differences in the size of the fine-crushed material and its distribution. Those produced by the circular sieve

were fine with a narrow particle distribution, whereas those by the elliptical sieve was relatively large (elongated shape) with wider distribution (Yamaguchi, et al., 2006).

4.2. *Driving conditions of the fine-crusher*

The values of *FD* and ASM_{135} obtained are shown in Table 2. The effect of distance from the digital camera to the sample (200 and 135 mm) was compared, although it should be ideally the same as for the photography discussed in the previous section (4.1). The multiple linear regression analysis (Table 4) demonstrated better fit and thus greater significance in the partial regression coefficients when images were taken at 135 mm than at 200 mm. The pore size of the punching sieve and the moisture content of material significantly affected the *FD* and the ASM_{135} at 135 mm distance.

Taking *FD* and ASM_{135} as intermediate ("bridging") parameters for circular and elliptical sieves, respectively, the smallest pore size of the punching sieve (1.5 mm) and the higher moisture content of material (70.1% d.b.) are the most favourable conditions for the fine-crusher leading to a high *LRI*. The higher rotor speeds (1750 rpm) is also the most favourable condition for the circular sieve. Although the effects of operating conditions on fractal dimension have been already reported (Yamaguchi et al., 2006), the effect of moisture content did not correspond with the results of this study.

Additional experiment. To discover the cause of this discrepancy, the contribution of moisture content to the complexity of the fine-crushed material was additionally investigated. Typical shapes of fine-crushed material observed under the scanning electron microscope are shown in Figure 2. Implicitly, the increase in the moisture content of the material induced complexity in the

fine-crushed material (from bottom left (a) to top right (b) in Fig. 2), leading to a high *LRI*.

The *FD* and the ASM_{135} was calculated for the fine-crushed material produced at 6 levels of moisture content (16.4%, 19.5%, 26.9%, 30.6%, 43.5% and 50.7% d.b.) with the 1.5 mm of circular or elliptical sieve. For the moisture contents of 16.4%, 30.6% and 50.7%, one gram of the sieved material (< 0.84 mm and > 0.54 mm) of circular sieve was manually divided into 3 types: (a) rounded, (b) ramified (see Fig. 2) and bark. This showed that the complexities of the shape of fine-crushed material increased with the moisture content of the material (Fig. 3a), and this was attributed to the increase in the portion of the exposed fibre of the material (Fig. 3b).

SEM analysis. The microscopic analysis on the scanning electron microscope (Fig. 4) revealed microscopic cracks around the surface of the fine-crushed material (Fig. 4 arrow M), and most of the cells by the surface were fractured along the cell wall interface (Fig. 4 arrow I). Since about 62% of the lignin is contained within intercellular layers and the primary wall (Asano, 1993), a high *LRI* of the ramified shape was attributed to the microscopic cracks and the fractures. Moreover, an increase in the moisture content of material facilitated the penetration of the subcritical water into the cells because the cracks and fractures deepen progressively as mentioned above, and the swelling property of wood cellulose, especially of the amorphous region, increased the removal of lignin because of the solubilisation of amorphous cellulose.

These observations confirmed that the high moisture content of the material contributed to an increase in both the complexity of the shape of the fine-crushed material and in the *LRI*. The activity of subcritical water around the vessels or on

the surface of fine-crushed material (Fig. 5 (c, circles) and (d)) demonstrated strong evidence of the removal of lignin contained mainly within intercellular layers and the primary wall (62% in volume) (Asano, 1993). The penetration of water into wood cells was also evidenced from Figure 5 (c). As demonstrated in Figure 3 (b), Figure 5 (d) indicates that very finely-crushed wood fibres are highly conducive to the removal of lignin.

5. Conclusions

The image characteristics of fine-crushed material produced by the fine-crusher that have a significant relationship to effective lignin removal are the fractal dimension of the green image for circular sieve and the angular second moment (135˚) of the brightness image for elliptical sieve. The performance of the fine-crusher has been optimized within the range of the present study to produce the most suitable shape of fine-crushed material leading to a high lignin removal index by the use of the smallest pore size of the punching sieve (1.5 mm) and the higher moisture content of material (70.1% d.b.). The fine-crushing for exposing the wood fibre increases the complexity of the material and results in a high lignin removal index.

Acknowledgments

This research was partially supported by the Ministry of Education, Science, Sports and Culture, Grant-in-Aid for Scientific Research (B), 16380169, 2004-2006.

References

Asano I (1993). Mokuzai no Ziten (Encyclopedia of Wood). Asakura, Tokyo, 76-78

Bodun P O; Shibusawa S; Sasao A; Sakai K (2000). Dredged sludge moisture prediction by textural analysis of the surface image. Journal of terramechanics, **37**, 3-20

Canneyt V T; Tijskens E; Ramon H; Verschoore R; Sonck B (2004). Development of a predictive tissue discolouration model based on electronic Potato impacts. Biosystems Engineering, **88** (1), 81–93

Forestry and Forest Products Research Institute (2004). Mokuzai kougyou handobukku (Wood industrial handbook). Maruzen, Tokyo, 965-979

Fujita Y; Takahashi S; Ueda M; Tanaka A; Okuda H; Morikawa Y; Kawaguchi T; Arai M; Fukuda H; Kondo A (2002). Direct and efficient production of ethanol from cellulosic material with a yeast strain displaying cellulolytic enzymes. Applied and Environmental Microbiology, **68**(10), 5136-5141

Fujita Y; Ito J; Ueda M; Fukuda H; Kondo A (2004). Synergistic saccharification, and direct fermentation to ethanol, of amorphous cellulose by use of an engineered yeast strain codisplaying three types of cellulolytic enzyme. Applied Environmental Microbiology, **70**(2), 1207-1212

Goto M; Obuchi R; Hirose T; Sakaki T; Shibata M; (2004). Hydrothermal conversion of municipal organic waste into resources. Bioresource Technology, **93**, 279-284.

Gregg D J; Boussaid A; Saddler J N (1998). Techno-economic evaluations of a generic wood-to-ethanol process. Bioresource Technology, **63**, 7-12

Haralick R M; Shanmugam K; Dinstein I (1973). Textural features for image classification. IEEE Transactions on systems, man, and cybernetics, **3**(6),

610-621

Hatano A; Horio H; Shoji K; Kawamura T (2002). Pre-processing technology for cellulose waste ethanolization. Proceedings of International Symposium on Automation and Mechatronics of Agricultural and Bioproduction Systems (ISMAB), 166-171

Hayashi N; Fujita S; Irie G; Sakaki T; Shibata M (2004). Reaction kinetics of Cellulose decomposition in hot-compressed-water. Journal of the Japan Institute of Energy, **83**, 805-814

Honda K (2002). Furakutaru (Fractal). Asakura, Tokyo, 42-45.

Image processing handbook edit committee (1987). Gazousyori handobullu (Image processing handbook). Shokodo, Tokyo, 295-303

Jain D; Pathare B P (2004). Selection and evaluation of thin layer drying models for infrared radiative and convective drying of onion slices. Biosystems Engineering, **89**(3), 289–296

The Japan Wood Research Society (2000). Mokusitu kagaku zikken manyuaru (Wood science experimental manual). Buneido, Tokyo, 93-94, 97

Magara K; Tsubouchi M; Koshijima T (1988). Change of pore-size distribution of lignocellulose by microwave irradiation. Mokuzai Gakkaishi, **34** (10), 858-862

Matsumura Y; Sudo K; Shimizu K (1977). Enzymatic hydrolysis of woods. II. Mokuzai Gakkaishi, **23** (11), 562-570

Pasini L; Ragni L; Rombolà D A; Berardinelli A; Guarnieri A; Marangoni B (2004). Influence of the fertilisation system on the mechanical damage of apples. Biosystems Engineering, **88** (4), 441–452

Sinício R (2004). Generalised longevity model for orthodox seeds. Biosystems

Engineering, **89** (1), 85–92

Sudo K; Matsumura Y; Shimizu K (1976). Enzymatic hydrolysis of woods. I. Mokuzai Gakkaishi, **22** (12), 670-676

Sun Y; Cheng J (2002). Hydrolysis of lignocellulosic materials for ethanol production: a review. Bioresource Technology, **83**, 1-11

Valero C; Ruiz-Altisent M; Cubeddu R; Pifferi A; Taroni P; Torricelli A; Valentini G (2004). Selection Models for the Internal Quality of Fruit, based on Time Domain Laser Reflectance Spectroscopy. Biosystems Engineering, **88** (3), 313–323

Yamaguchi D; Horio H; Shoji K; Kawamura T; Itoh H (2004). Pre-processing technology for wood-based cellulose ethanolization. Proceedings of International Symposium on Automation and Mechatronics of Agricultural and Bioproduction Systems (ISMAB), S3-2A73 (CD-ROM)

Yamaguchi D; Shoji K; Kawamura T; Itoh H; Horio H (2006). Preprocessing technology for ethanol production from wood-cellulosic materials (Part 1). Journal of Japanese Society of Agricultural Machinery, **68** (6), 91-100

Figure captions

Fig. 1 - Flowchart of image processing.

Fig. 2 - Scanning electron microscope images of typical shapes of fine-crushed material (before subcritical water treatment); (a) rounded and (b) ramified shape.

Fig. 3 - Effects of moisture content of material on (a) fractal dimension (filled) and angular second moment (135˚) (unfilled), (b) transition of component (rounded, ramified (Fig. 2) and bark) of sieved material (<

0.84 mm and > 0.54 mm, 1 g).

Fig. 4 - Section of fine-crushed material (scanning electron microscope image, before subcritical water treatment): I, intercellular fracture; M, microscopic crack.

Fig. 5 - Scanning electron microscope images of fine-crushed material ((a) and (b): untreated; (c) and (d): treated with subcritical water): treatment temperature, 220˚C; treatment time, 10 min; fractal dimension, 1.944 (a, c) and 1.949 (b, d); slurry concentration, 1%.

Figure 1

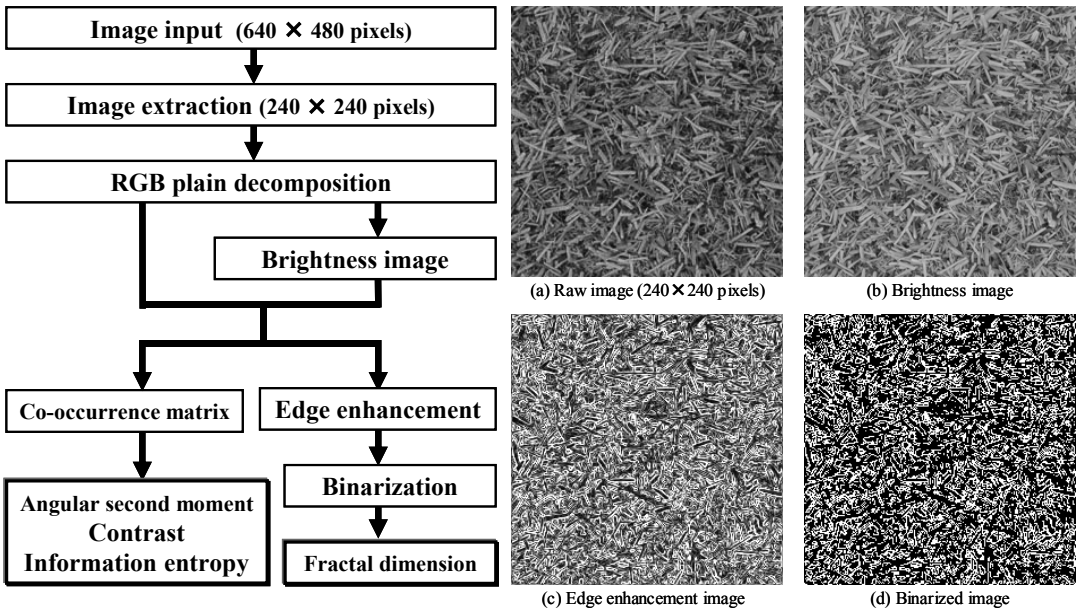

Fig. 1 - Flowchart of image processing.

Figure 2

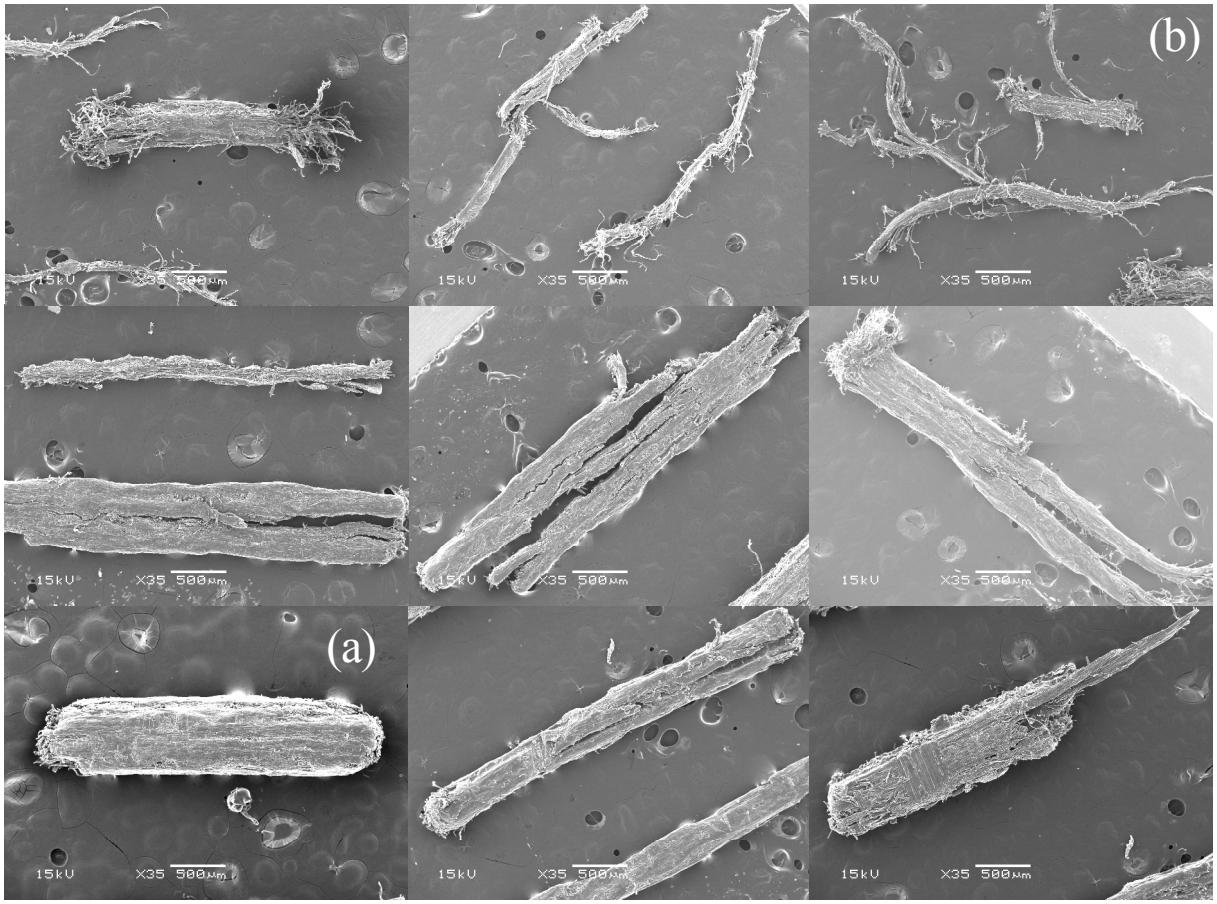

Fig. 2 - Scanning electron microscope images of typical shapes of fine-crushed material (before subcritical water treatment); (a) rounded and (b) ramified shape.

Figure 3

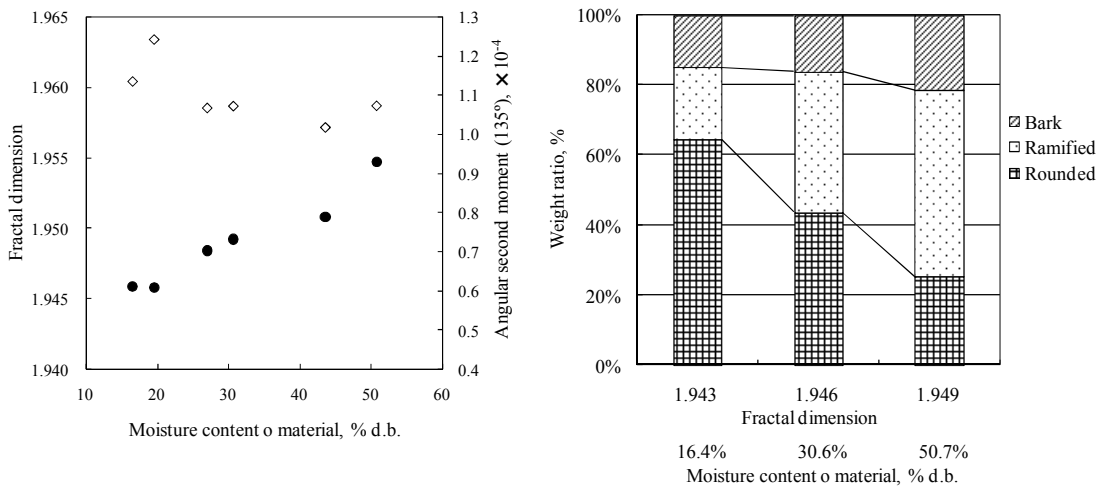

(a) (b)

Fig. 3 - Effects of moisture content of material on (a) fractal dimension (filled) and angular second moment (135°) (unfilled), (b) transition of component (rounded, ramified (Fig. 2) and bark) of sieved material (< 0.84 mm and > 0.54 mm, 1 g).

Figure 4

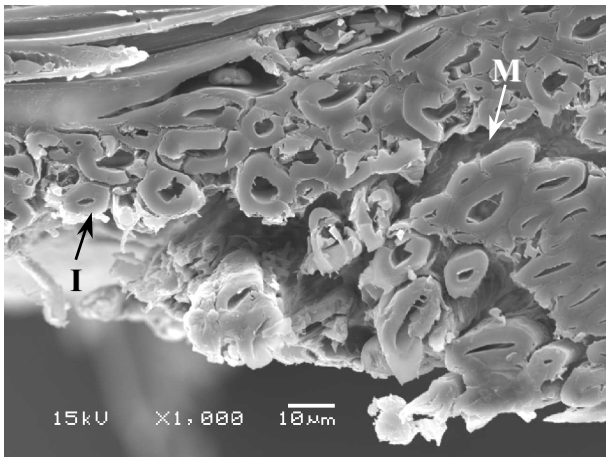

Fig. 4 - Section of fine-crushed material (scanning electron microscope image, before subcritical water treatment): I, intercellular fracture; M, microscopic crack.

Figure 5

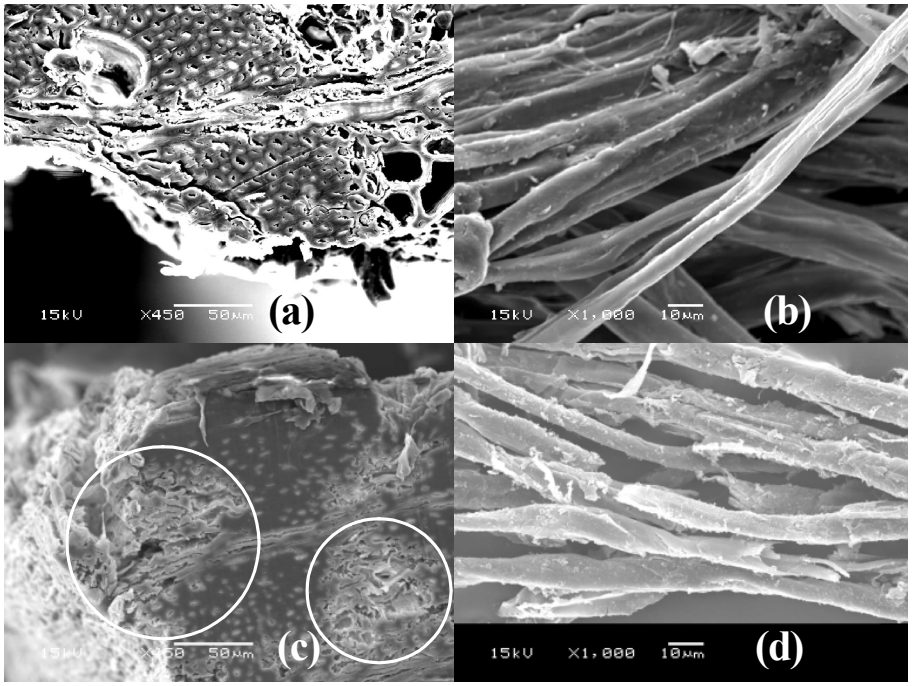

Cross-section (×450) Surfaces of wood fibers (×1000)

Fig. 5 - Scanning electron microscope images of fine-crushed material ((a) and (b): untreated; (c) and (d): treated with subcritical water): treatment temperature, 220˚C; treatment time, 10 min; fractal dimension, 1.944 (a, c) and 1.949 (b, d); slurry concentration, 1%.

Table 1

Table 1 - Lignin removal index associated with the driving conditions of fine-crusher[1].

Sample No.	Pore shape	Property of sieve 1	Property of sieve 2	Rotor speed, rpm	Sieve speed[5], rpm	Lignin removal index, % (Two replicates)	
		Pore axis[2]	ORE[4]			I	II
1	Elliptical (−)	Parallel (−)	22.5% (−)	1250 (−)	−30 (−)	21.9	2.8
2	Elliptical (−)	Parallel (−)	40.3% (+)	1750 (+)	30 (+)	16.0	−12.0
3	Elliptical (−)	Vertical (+)	22.5% (−)	1750 (+)	30 (+)	26.2	−2.0
4	Elliptical (−)	Vertical (+)	40.3% (+)	1250 (−)	−30 (−)	11.3	−15.9
		ORC[3]	(Error)				
5	Circular (+)	22.7% (−)	(−)	1250 (−)	30 (+)	22.4	17.7
6	Circular (+)	22.7% (−)	(+)	1750 (+)	−30 (−)	22.5	16.8
7	Circular (+)	40.3% (+)	(−)	1750 (+)	−30 (−)	9.6 [6]	12.0
8	Circular (+)	40.3% (+)	(+)	1250 (−)	30 (+)	25.7	9.1

(−) and (+) indicate LOW and HIGH levels of each factor

1) Experimental parameters and levels were assigned to an orthogonal array L_8
   Moisture content of material: 12.3% d.b.
   Feeding rate of material: 10 g s^{-1}

2) Direction of the major axis of the elliptical pores to the rotor shaft

3) Opening ratio of the circular-pore punching sieve
   22.7%: $D \times P = 2 \times 4$ mm; 40.3%: $D \times P = 2 \times 3$ mm (Yamaguchi et al., 2006)

4) Opening ratio of the elliptical-pore punching sieve
   22.5%: $W \times L \times S_p \times L_p = 2 \times 10 \times 5 \times 17$ mm; 40.3%: $W \times L \times S_p \times L_p = 3 \times 20 \times 6 \times 24$ mm (Yamaguchi et al., 2006)

5) Negative sign for the reverse direction to the rotation of the rotor

6) An outlier

Table 2

Table 2 - Fractal dimension and angler second moment (135˚) associated with the driving conditions of fine-crusher

Parameters					Circular sieve		Elliptical sieve	
Pore size,[1),2)] mm	Moisture content of material, % d.b.	Rotor speed, rpm	Feeding rate of material, g s^{-1}	Sieve speed,[3)] rpm	Fractal dimension (Green image)		Angular second moment (135˚) $\times 10^{-4}$ (Brightness image)	
					200 mm[4)]	135 mm[4)]	200 mm[4)]	135 mm[4)]
1.5	15.5	1250	10	−30	1.962	1.946	0.927	1.231
1.5	15.5	1500	15	0	1.962	1.949	0.938	1.234
1.5	15.5	1750	20	30	1.964	1.948	0.933	1.252
1.5	47.1	1250	15	30	1.961	1.946	0.915	1.118
1.5	47.1	1500	20	−30	1.961	1.953	0.900	1.229
1.5	47.1	1750	10	0	1.962	1.947	0.966	1.242
1.5	70.1	1250	20	0	1.954	1.955	1.210	1.208
1.5	70.1	1500	10	30	1.955	1.953	1.150	1.154
1.5	70.1	1750	15	−30	1.954	1.955	1.190	1.200
2.0	15.5	1250	10	30	1.953	1.920	1.000	1.299
2.0	15.5	1500	15	−30	1.956	1.920	0.984	1.287
2.0	15.5	1750	20	0	1.954	1.926	0.949	1.267
2.0	47.1	1250	15	0	1.953	1.926	0.896	1.217
2.0	47.1	1500	20	30	1.954	1.933	0.915	1.135
2.0	47.1	1750	10	−30	1.955	1.932	0.964	1.187
2.0	70.1	1250	20	−30	1.955	1.944	1.190	1.189
2.0	70.1	1500	10	0	1.954	1.939	1.190	1.167
2.0	70.1	1750	15	30	1.954	1.941	1.130	1.109
3.0	15.5	1250	10	0	1.938	1.889	1.110	1.435
3.0	15.5	1500	15	30	1.940	1.891	0.991	1.537
3.0	15.5	1750	20	–30	1.947	1.896	1.050	1.627
3.0	47.1	1250	15	–30	1.938	1.900	1.140	1.411
3.0	47.1	1500	20	0	1.943	1.907	1.120	1.521
3.0	47.1	1750	10	30	1.939	1.913	1.070	1.445
3.0	70.1	1250	20	30	1.944	1.909	1.180	1.465
3.0	70.1	1500	10	–30	1.940	1.915	1.050	1.308
3.0	70.1	1750	15	0	1.945	1.922	1.150	1.453

1) The circular-pore punching sieve (opening ratio: 40.3%),
$D \times P$ = 1.5×2.25 mm ; 2.0×3.0 mm; 3.0×4.5 mm (Yamaguchi et al., 2006)

2) The elliptical-pore punching sieve (opening ratio: 22.5%),
$W \times L \times S_p \times L_p$ = 1.5×25×5.5×30 mm; 2.0×10×5.0×17 mm; 3.0×20×10×26 mm (Yamaguchi et al., 2006)

3) Negative sign for the opposite direction to the rotation of the rotor

4) A distance between a distal camera and a sample

Table 3

Table 3 - Significant partial regression coefficients of selected image characteristics related to lignin removal index.

Circular sieve

Image	Selected image characteristics		R^2_{adj} [1)]	P-value [2)]
	FD	*CV*		
Brightness	0.951 ***		0.89	0.0010
Red	0.954 ***		0.89	0.0009
Green	0.963 ***		0.91	0.0005
Blue		0.805 *	0.58	0.0288

Elliptical sieve

Image	Selected image characteristics		R^2_{adj} [1)]	P-value [2)]
	ASM_{135}	IE_{135}		
Brightness	−0.971 ***		0.93	< 0.0001
Red	−0.966 ***		0.92	< 0.0001
Green	−0.967 ***		0.92	< 0.0001
Blue		0.950 ***	0.89	0.0003

FD denotes the fractal dimension, *CV* the contrast variance, ASM_{135} the angular second moment (135°), IE_{135} the information entropy (135°)

*, **, ***; significance levels of 5%, 1% and 0.1%, respectively in tow-side *t*-test

1) Squared multiple correlation coefficients adjusted for the degrees of freedom of the model

2) Observed significance level of the test

Table 4

Table 4 - Significant partial regression coefficients between selected image characteristics and the driving conditions of the fine-crusher.

Parameters	Circular sieve *FD* (Green image)		Elliptical sieve ASM_{135} (Brightness image)	
	200 mm [1]	135 mm [1]	200 mm [1]	135 mm [1]
Pore size	−0.93 ***	−0.91 ***	0.33 *	0.83 ***
Moisture content of material	NS	0.33 ***	0.63 ***	−0.31 **
Rotor speed	NS	0.10 *	NS	NS
Feeding rate of material	NS	NS	NS	NS
Sieve speed	NS	NS	NS	NS
R^2_{adj} [2]	0.87	0.95	0.47	0.77
P-value [3]	< 0.0001	< 0.0001	0.0002	< 0.0001

FD denotes the fractal dimension, ASM_{135} the angular second moment (135°)
*, **, ***; significance levels of 5%, 1% and 0.1%, respectively in tow-side *t*-test
"NS" denotes an insignificant parameter
1) A distance between a distal camera and a sample
2) Squared multiple correlation coefficients adjusted for the degrees of freedom
3) Observed significance level of the test